Received: 1 October 2020 | Revised: 12 November 2020 | Accepted: 13 November 2020

DOI: 10.1111/rge.12253

ORIGINAL ARTICLE

RESOURCE GEOLOGY WILEY

Significance of radioelements distribution in the Precambrian rocks of Jabel Sayid, western Saudi Arabia, using spectrometric and geochemical data

Hamdy H. Abd El-Naby[1] | **Yehia H. Dawood**[2] | **Abduallah A. Sabtan**[1] | **Mahmood S. Al Yamani**[1]

[1]Faculty of Earth Sciences, King Abdulaziz University, Jeddah, Saudi Arabia

[2]Department of Geology, Faculty of Science, Ain Shams University, Cairo, Egypt

Correspondence
Hamdy H. Abd El-Naby, Faculty of Earth Sciences, King Abdulaziz University, P.O. Box 80206, Jeddah 21589, Saudi Arabia.
Email: hhabdel@yahoo.com

Funding information
King Abdulaziz City For Science And Technology (KACST), Grant/Award Number: AT-30-31

Abstract

In situ gamma-ray spectrometry measurements were carried out using RS-230 BGO spectrometer over an area of 9.4 km^2. One hundred and seventy eight spectrometric points were collected along parallel profiles with spacing 325 m in the Easting X direction and Northing Y direction. The results are treated statistically to determine the minimum, maximum, arithmetic mean (X), *SD* (S), and coefficient of variability (CV %). The spectrometric survey revealed the presence of radioactive zones in the aplite-pegmatite with maximum eU content of 1,550 ppm and eTh of 7,974 ppm, whereas alkali granite has an average eU content of 12 ppm and eTh of 34 ppm. Felsite has an average eU and eTh close to that of alkali granite, 11 and 32 ppm, respectively. Pegmatite veins cutting alkali granite have high values of eU and eTh, an average of 34 and 101 ppm, respectively. The metamorphosed volcanic rocks of the Mahd Group demonstrate the lowest radioactivity with an average eU content of 0.8 ppm and eTh of 1.6 ppm. These rocks partly show evidences of post-magmatic alteration processes, for example, silicification, sericitization, and oxidation. Excluding metavolcanics, the strong positive correlation between eU and eTh for the different rock varieties reflects their geochemical coherence during magma crystallization and indicates that both elements are largely accommodated into accessory minerals and were not disturbed by alteration. The CV values of the different rock units show normal distribution, where all the percentages of CV values are less than 100, with the exception of eU of felsite that shows CV % value slightly higher than 100. The aplite-pegmatite, alkali granite, and the associated pegmatite veins show negative value of uranium outward migration, but are still the most favorable host rocks for uranium and thorium mineralization. A tentative interpretation of such contradiction suggests that uranium is largely accommodated into accessory minerals and only limited labile uranium redistribution has occurred and uranium was precipitated in association with alteration products. This interpretation is supported by the presence of kasolite $Pb(UO_2)SiO_4.(H_2O)$, along the fractured zones and quartz veins in the aplite-pegmatite. The limited uranium migration in the

study area was also revealed by the low weathering rate estimated by the calculations of chemical indices of alteration.

KEYWORDS

alkali granite, aplite-pegmatite, gamma-ray spectrometry, Sayid, uranium migration, weathering indices

1 | INTRODUCTION

In 2017, The Saudi Geological Survey has started a survey to explore and assess uranium and thorium resources in Kingdom of Saudi Arabia. The project is carried out in cooperation with the King Abdullah City for Atomic and Renewable Energy (KACARE) and the China National Nuclear Corporation (CNNC). In this paper, we present a contribution to the U-Th exploration activity in Saudi Arabia using ground gamma-ray spectrometric survey. For more than 50 years, gamma-ray spectrometry has been used to detect radioactive sources, map rocks and soils, find hydrocarbon and mineral deposits, and monitor environmental hazards (Shives, 2017; Hamath Ba *et al*., 2020). Gamma-rays emitted from the ground surface are related to the primary mineralogy, geochemistry of the bedrock, and the weathered materials.

Most of the radioactive occurrences in the Arabian Shield of Saudi Arabia are present in alkali granite and associated pegmatite. This association has been subjected earlier to metasomatic processes (Dawood *et al*., 2014). These rocks contain considerable amounts of heavy minerals, such as ilmenite, magnetite, garnet, monazite, zircon, rutile, pyrite, siderite, sphalerite, and titanite. In addition to U-Th bearing accessory minerals, such as thorite and pyrochlore. Previous studies indicated the occurrence of uranium mineralization and associated elements, such as Th, Nb, Ta, Pb, Y, Zr, and REE in many areas of Arabian Shield of Saudi Arabia (Küster, 2009). Jabel Sayid represents an important occurrence for radioelements and heavy metals (Drysdall and Douch, 1986).

The genetic relationship between granite intrusions and associated uranium mineralization has been discussed for a long time. Uranium in granites can be genetically divided into two groups; primary uranium and secondary uranium (Jiashu and Zehong, 1982). The former is fixed in rocks during the crystallization of magma, while the latter is precipitated from circulating fluids carrying dissolved uranium. The secondary uranium can be subdivided into three types; (a) Adsorbed uranium on alteration products such as montmorillonite, chlorite, and limonite; (b) Interstitial uranium at the grain boundaries which was formed as a result of hydrothermal solution moving along the interstices of minerals in granites, and (c) Precipitated uranium in microfractures and cavities due to evaporation of solutions. These three types of secondary uranium are regarded as the final preserved products through all the geological processes such as metasomatism, hydrothermal alteration, and weathering.

Uranium mineralization in Jabel Sayid is associated with high concentrations of Nb and REEs (Turkistany and Ramsay, 1982). Uranium contents vary between 49 and 134 ppm (Hackett, 1986). Dawood *et al*. (2010) reported the presence of kasolite [$Pb(UO_2)SiO_4$-(H_2O)] as a main uranyl mineral in the aplite-pegmatite of Jabel Sayid. It commonly forms clusters of yellow acicular crystals in the voids and fractures. U-series isotopic composition indicates that secondary uranium mineralization in Jabel Sayid is characterized by high $^{230}Th/^{234}U$ and $^{230}Th/^{238}$ U activity ratios. Conversely, the low $^{234}U/^{238}U$ activity ratio of this mineralization is indicative of enhanced groundwater circulation at the time of mobilization and reprecipitation (Dawood *et al*., 2014).

Ground gamma-ray spectrometry is one of the important means to assist uranium exploration. Generally, the results of a gamma-ray spectrometry survey are presented as maps of potassium K (%), equivalent uranium eU (ppm), equivalent thorium eTh (ppm), total dose rate (nGy/h), and ratios of eU/eTh, eU/K, and eTh/K (IAEA, 2010). The main objectives of this paper are therefore:

1. To determine the surface concentrations of radioelements (K, U, and Th) in the granitic intrusions of Jabel Sayid.
2. To analyze the trends and the behavior of eU, eTh, and their ratios as an indicator of uranium remobilization to evaluate the redistribution of radioactive elements in the study area.
3. To apply uranium migration concepts to the ground gamma-ray spectrometric data in order to follow and localize radioactive anomalies in the study area.
4. To use uranium favorability indices U_1 and U_2, and other geochemical parameters to estimate the degree of migrated uranium, in and out of the rock units, and favorable sites of potential radioelement concentrations in Jabel Sayid area.

5. To use three known weathering indices, Chemical Index of Alteration, Chemical Index of Weathering and Plagioclase Index of Alteration (Nesbitt and Young, 1982; Harnois, 1988; Fedo *et al*., 1995) to identify the role of chemical weathering and alteration in the leaching and transporting of uranium.

2 | FIELD GEOLOGY AND PETROGRAPHY

Jabel Sayid area is located at the western part of Saudi Arabia (Figure 1). The area is composed of igneous and metamorphic rocks of Pre-cambrian age. The study area is covered mainly by volcano-sedimentary rocks of the Mahd Group and granitic rocks (Pellaton, 1981; Coleman *et al*., 1983; Moufti, 1985; Camp and Roobol, 1989).

The Mahd Group consists of metamorphosed basalt, basaltic andesite, andesite, dacite, rhyolite lavas, pyroclastic rocks, with subordinate amounts of sandstone, siltstone, pebble conglomerate, and minor limestone, some of which were deposited in a subaerial environment. These rocks are economically important as host for the Jabel Sayid volcanic-massive sulfide deposits and the Mahd adh Dhahab epithermal gold deposit (Luce *et al*., 1979). The age of these rocks varies between 775 and 785 Ma (Hargrove, 2006). The metamorphosed dacite of the Mahd Group consists of quartz, feldspar, amphibole, and biotite (Figure 2a), in addition to the presence of some accessory minerals such as zircon (Figure 2b). Andesite contains calcite veins and show microfolding deformation. It is composed mainly of hornblende and plagioclase (Figure 2c,d).

Alkali granites intrude the late Proterozoic volcanosedimentary rock unit of the Mahd Group. These granites reflect a Rb/Sr age of 584 ± 26 Ma (Calvez *et al*., 1983). Zircon U–Pb isotopic dating revealed that the alkali granites have Ediacaran age (593 Ma), which is similar to many post-collisional alkali granites in the Arabian Nubian Shield (Moghazi *et al*., 2015).

This granitic rock is considered as the chilled carapace of typical Arabian Shield alkali granites (Hackett, 1986). It is part of the Jabel Hadb ash Sharar complex, which comprises a core of pink monzogranite surrounded by a broad zone of gray hornblende-biotite monzogranite to granodiorite. Two varieties of alkali granites of the Jabel Sayed pluton are recognized. The first variety is named as oxidized alkali granite that has sharp intrusive contacts with the aplite-pegmatite body (Figure 3b). Numerous dikes and veins invade joints and fractures parallel to this contact. The oxidized alkali granite is fine grained and shows signs of metasomatic effect. Centimetric to metric pegmatite veins, quartz veins, cavities, and vugs are occasional. The second variety is coarse to medium-grained massive alkali granite with no signs of metasomatic effect. This is the main variety, identified in the southern part of the pluton. The mineral composition of this granite is dominated by quartz, microcline, plagioclase, biotite, aegirine, and riebeckite (Figure 3a). Accessory minerals such as zircon, apatite, ilmenite, and fluorite are observed.

The Jabel Sayid aplite-pegmatite body lies along the northern margin of the alkali granite pluton of Jabel Sayid (Figure 3b). The aplite-pegmatite is a sheet-like body with a strike length of about 2 km (Turkistany, 1979). The main aplite-pegmatite crops out almost continuously for about 1 km (Figure 1) and dips 45° to 75° north. Depending on iron oxide contents, the color of this aplite-pegmatite body shows buff and pink, to darker red and brown in color; in addition to uncommon black color. According to Hackett (1984), the internal structure

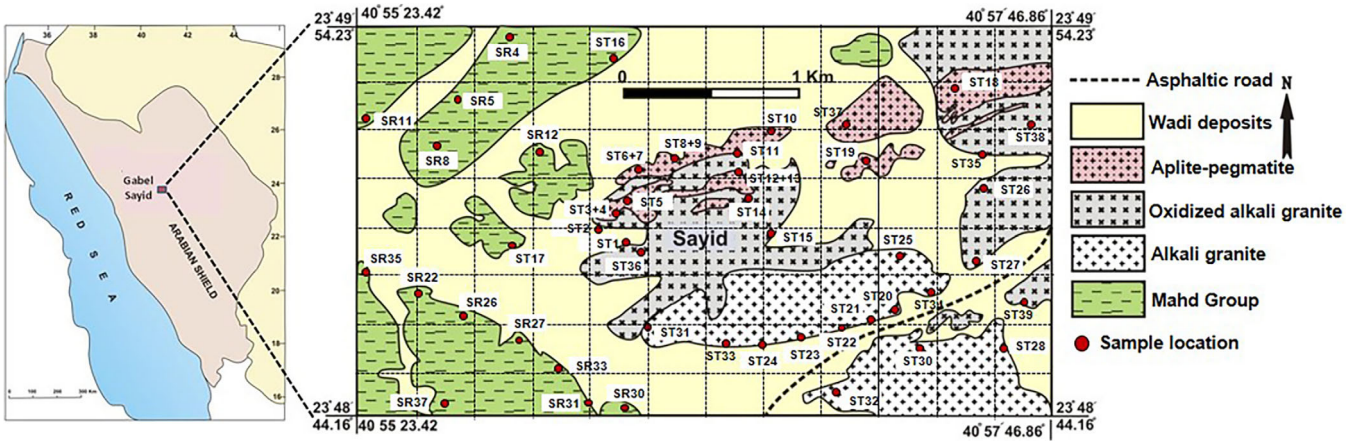

FIGURE 1 Geological map of the Jabel Sayid area, Saudi Arabia. Horizontal and vertical dashed lines represent the grid pattern for spectrometric measurements over the different lithologies

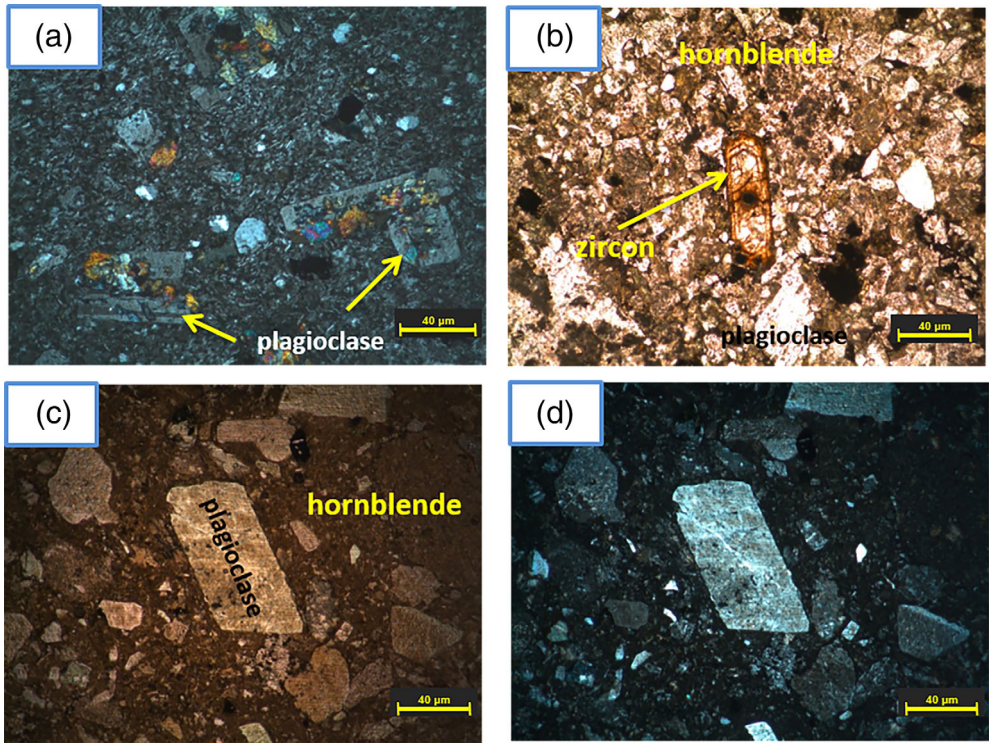

FIGURE 2 Photomicrographs of the metamorphosed volcanic rocks of the Mahd Group. (a) Metamorphosed dacite under crossed polars. (b) Zircon in metamorphosed dacite under plane polarized light. (c,d) Metamorphosed andesite under plane polarized light and crossed polars

of the aplite-pegmatite is layered and varied in composition. The layers are 0.3–5.0 m thick and consist of micropegmatite and aplite, of which crystals are up to 3 cm long. The coarse-grained aplite-pegmatite is composed mainly of microcline, plagioclase, and quartz (Figure 3c). Many felsite dikes (about 1–3 m thick) cut the granitic rocks of Jabel Sayid (Figure 3d). Petrographically, felsites are composed mainly of K-feldspar, plagioclase, and quartz (Figure 3e).

3 | METHODOLOGY

3.1 | Spectrometric survey

In this study, in situ gamma-ray spectrometry measurements were carried out using a RS-230 BGOSuper-SPEC spectrometer model of Radiation Solution Inc, with a Bismuth Germanate Oxide (BGO) crystal detector that makes it also an ideal portable instrument for potassic alteration measurements. Within the detector, an internal ^{137}Cs source allows the spectrometer to automatically maintain system gain stability. The accuracy of the measurements was provided by the system of spectrum stabilization through a digital circuitry. The factory calibration of the gamma-ray spectrometer was made to high volume standards for each element ^{238}U, ^{232}Th, and ^{40}K and for background. To improve results, two measurements from the same site were performed. These replicate measurements provided an error less than 5% for K, U, Th, and total dose rate.

Detailed spectrometric measurements over the different lithologies were carried out along an equal grid, with spacing 325 m in the Easting X direction and Northing Y direction with an increase of the grid stations to about 50 m spacing on the areas showing high recordings (Figure 1). The spectrometer was placed very close to the ground, with a sample time of 120 s. All data were recorded, stored, and compiled both manually in the field notebook and electronically in the memory storage of the device. The ^{40}K concentration was measured in mass percentage (%) because of its higher crustal abundance, while ^{238}U and ^{232}Th in equivalent parts per million (eU and eTh), which indicates that their concentrations were inferred from daughter elements in their decay chains. The total gamma activity of rocks can be judged by means of dose rate measurement in nGy/h, which is based on the evaluation of the total spectral count.

IBM SPSS statistical program, version 24, was used to do certain statistical analysis such as mean value (X), *SD* (S), coefficient of variability (CV = S/X × 100), as well as determination of the minimum and maximum values for the different gamma-ray spectrometric variables (Table 1). The coordinates from the Garmin GPS were entered and all spectrometric data corresponding to those coordinates were imported into SURFER 8.0, allowing contour maps to be plotted with the data. Inverse distance interpolation method is preferred over the other

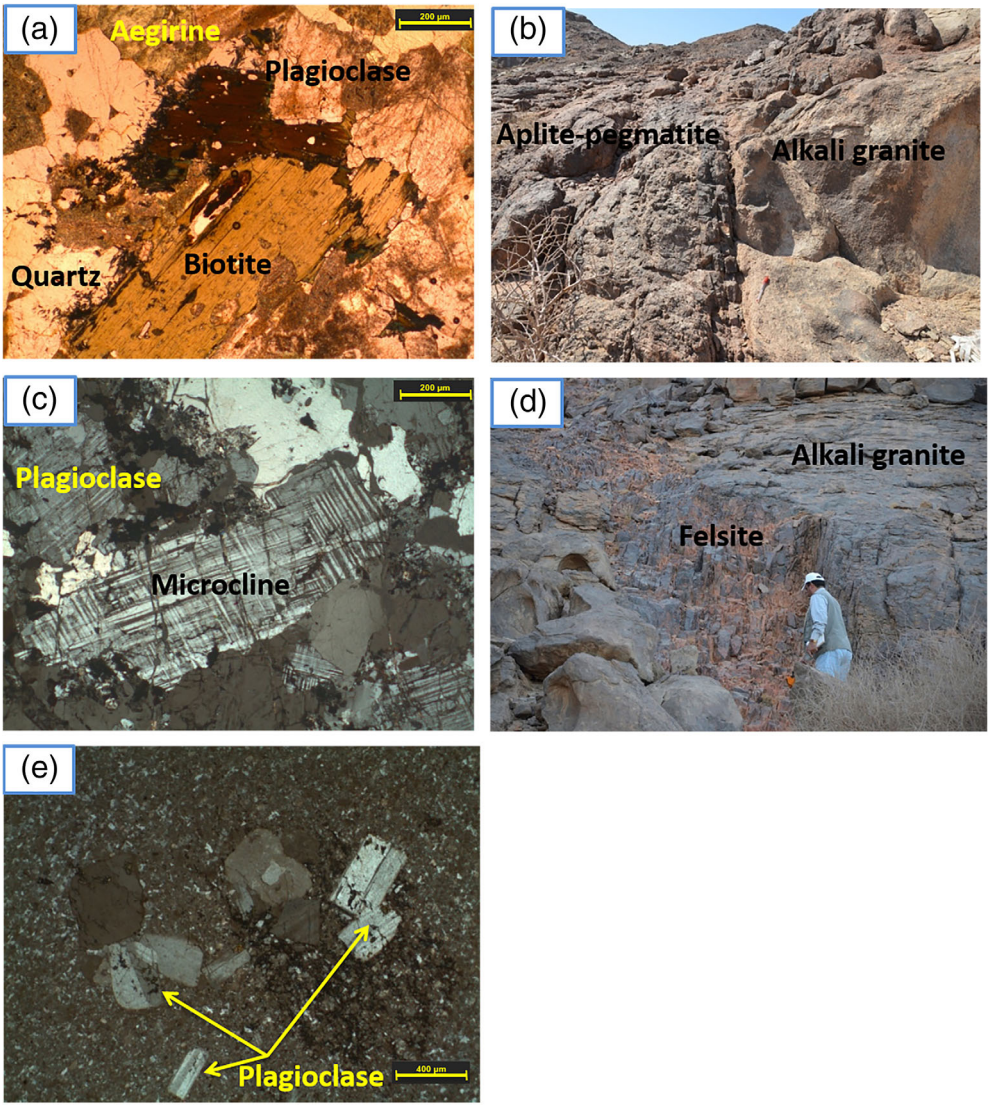

FIGURE 3 (a) Photomicro graph of alkali granite under plane polarized light. (b) Contact between alkali granite and aplite-pegmatite of Jabel Sayid. (c) Photomicro graph of the aplite-pegmatite under crossed polars. (d) Felsite dike in alkali granite. (e) Photomicrograph of the felsite under crossed polars

geostatistical techniques. The robustness and simplicity of inverse distance interpolation motivate its use in the present paper. Moreover, the inverse distance estimates become smoother with increase in the number of data for the same exponent value.

3.2 | Geochemical analysis

Major elements of 62 rock samples were analyzed using X-Ray Fluorescence (XRF) at the laboratories of the Acme Labs, Canada. The Loss On Ignition (LOI) has been measured by burning the sample at about 450°C for 6 hr. The sample was then put into a crucible of platinum-gold where it was melted down with lithium tetraborate. Molten material was placed in a special mold of platinum and analyzed later by X-Ray Fluorescence machine. The results of the chemical analyses are given in Table 2.

4 | RESULTS AND DISCUSSIONS

4.1 | Gamma-ray Spectrometric study

4.1.1 | Radioelements distribution and characterization

Results of the gamma-ray spectrometric survey of Jabel Sayid pluton are illustrated in the form of contour maps (Figure 4). In general, the radioelement distribution shows that the high concentrations of radioelements are related to aplite-pegmatite and alkali granite. From the total dose rate contour map (Figure 4a), the lithologies of granitic rocks can be easily distinguished from that of metavolcanics of the Mahd Group. Three main anomalous zones could be noticed (>5,000 nGyh-1). These zones are restricted to areas of aplite-pegmatite, where several pegmatite and quartz veins, about 5–50 m long and 0.2–1 m wide, are observed. Total dose rate readings

TABLE 1 Statistical results of gamma-ray spectrometric analyses of the study area

Aplite-pegmatite						
	N	**Minimum**	**Maximum**	**X**	**S**	**CV%**
Total dose rate ($nGyh^{-1}$)	64	256	27,900	7,773	6,640	85.43
eTh (ppm)	64	27.50	7,974	1,841	1,839.70	99.93
eU (ppm)	64	17.40	1,550	488.42	387.87	79.41
K (%)	64	3.30	62.3	16.83	15.10	89.76
eU/eTh	64	0.13	1.27	0.43	0.31	
eU/K	64	5.27	81.60	32.68	17.14	
Alkali granite						
Total dose rate (nGyh-1)	56	100	628	205	93.08	45.31
eTh (ppm)	56	11	126	33.80	20.65	61.08
eU (ppm)	56	5.1	42	12.43	6.77	54.43
K (%)	56	1.4	4.9	3.72	0.73	19.65
eU/eTh	56	0.2	0.94	0.39	0.14	
eU/K	56	1.21	11.9	3.59	2.40	
Wadi deposits close to aplite-pegmatite and alkali granite						
Total dose rate (nGyh-1)	16	45	3,800	698.13	1,082.9	155.12
eTh (ppm)	16	4.9	1,051	161.17	305.19	189.36
eU (ppm)	16	1.8	164	34.18	49.36	144.4
K (%)	16	1.10	4.20	2.54	1.05	41.15
eU/eTh	16	0.16	3.56	0.49	0.82	
eU/K	16	0.85	40	9.99	11.98	
Pegmatite veins in alkali granite						
Total dose rate (nGyh-1)	8	191	1,300	510.75	420.52	82.33
eTh (ppm)	8	19.3	272.9	101.14	94.45	93.39
eU (ppm)	8	10	96.4	33.74	32.03	94.93
K (%)	8	4.1	5.9	4.63	0.6	12.91
eU/eTh	8	0.13	0.8	0.4	0.2	
eU/K	8	2.44	16.34	6.79	5.49	
Felsite dikes						
Total dose rate ($nGyh^{-1}$)	20	107	578.	197.4	113.29	57.39
eTh (ppm)	20	16.4	93	32.35	19.58	60.54
eU (ppm)	20	2.8	50	10.95	11.29	103.13
K (%)	20	0.10	5.4	3.87	1.18	30.49
eU/eTh	20	0.17	0.55	0.31	0.11	
eU/K	20	0.76	110.00	8.10	24.12	
Metavolcanics						
Total dose rate ($nGyh^{-1}$)	13	7.1	49	22.64	14.03	61.97
eTh (ppm)	13	0.1	4.3	1.61	1.23	76.40
eU (ppm)	12	0.1	2	0.84	0.56	66.66
K (%)	13	0.2	2	0.92	0.62	67.39
eU/eTh	13	0.07	8	0.49	2.09	
eU/K	13	0.33	2	1.09	0.56	

TABLE 2 Major elements chemistry of the samples from Jabel Sayid area

Sample No.		LOI	SiO_2	Al_2O_3	Fe_2O_3	CaO	MgO	Na_2O	K_2O	MnO	TiO_2	P_2O_5	Cr_2O_3	SUM	CIA	CIW	PIA
Unit		%	%	%	%	%	%	%	%	%	%	%	%	%			
MDL	Analyte	−5.11	0.1	0.01	0.01	0.01	0.01	0.01	0.01	0.01	0.01	0.01	0.001	0.01			
ST 5	Aplite-pegmatite	4.88	75.8	9.10	2.25	1.66	0.03	0.38	4.95	0.01	0.09	0.01	0.027	99.19	51.64	73.43	54.06
ST 6		1.43	75.3	11.85	3.69	0.80	0.04	0.21	4.86	0.01	1.35	0.01	0.020	99.57	62.77	86.83	78.81
ST 7		3.38	73.6	10.33	2.73	2.62	0.08	0.34	4.89	0.01	1.13	0.11	0.039	99.26	49.98	66.02	49.96
ST 8		3.90	72.6	8.48	6.52	2.49	0.04	0.42	3.55	0.01	0.72	0.01	0.029	98.77	48.44	61.93	47.23
ST 9		1.76	76.6	10.17	4.81	0.71	0.04	0.22	4.97	0.01	0.52	0.01	0.042	99.86	59.23	86.03	74.68
ST 10		3.02	72.9	9.45	4.64	4.01	0.07	0.27	4.16	0.01	0.49	0.12	0.027	99.17	44.19	55.02	39.97
ST 11		2.47	71.5	10.01	7.09	1.78	0.04	0.24	4.40	0.21	0.32	0.09	0.031	98.18	55.07	73.40	60.63
ST 12P		2.27	75.2	10.27	3.26	1.37	0.06	0.97	5.78	0.01	0.40	0.01	0.031	99.63	49.91	71.56	49.78
ST 14F		2.48	71.1	10.43	4.49	2.02	0.06	0.32	7.60	0.02	0.58	0.04	0.024	99.16	45.86	71.32	35.09
ST 18		2.57	74.9	11.71	3.85	1.50	0.14	0.26	4.31	0.08	0.36	0.51	0.050	100.24	63.99	78.80	78.50
ST 13	Alkali granite	0.87	74.9	10.61	3.60	0.73	0.03	4.06	3.87	0.06	0.16	0.01	0.022	98.94	46.61	57.02	44.63
ST 14G		0.58	74.4	11.33	3.61	0.60	0.08	5.46	3.59	0.05	0.07	<0.01	0.017	99.81	44.88	52.97	42.60
ST 15		3.66	74.5	9.50	3.55	0.83	5.78	0.71	0.77	0.08	0.15	0.01	0.021	99.51	73.18	78.04	76.59
ST 19		0.76	74.0	11.02	3.88	0.66	0.11	5.31	3.78	0.05	0.10	0.01	0.010	99.70	44.07	52.62	41.19
ST 20		0.38	75.0	11.02	3.87	0.29	0.02	5.06	4.04	0.04	0.07	0.03	0.019	99.87	45.62	55.49	43.14
ST 21		0.46	75.6	12.92	1.27	0.67	0.16	4.59	4.35	0.09	0.09	0.01	0.016	100.23	49.02	59.60	48.48
ST 22		1.16	72.9	13.48	1.84	1.41	0.52	5.55	2.30	0.03	0.24	0.08	0.019	99.57	49.10	53.58	48.90
ST 23		0.38	74.8	10.99	3.91	0.22	0.03	5.30	4.02	0.05	0.10	<0.01	0.012	99.79	45.01	54.68	42.25
ST 24		0.40	75.5	10.64	4.94	0.15	0.02	4.03	3.88	0.02	0.11	<0.01	0.023	99.71	49.02	60.68	48.41
ST 28		0.34	75.2	10.70	3.63	0.18	0.02	5.01	4.24	0.05	0.07	<0.01	0.007	99.44	44.92	55.56	41.75
ST 30G		0.58	75.5	10.42	4.40	0.42	0.04	4.28	3.97	0.05	0.08	<0.01	0.005	99.71	46.35	57.21	44.09
ST 31A		0.47	76.1	11.21	3.69	0.19	0.04	4.31	3.66	<0.01	0.07	0.05	0.004	99.80	49.88	60.15	49.82
ST 31B		1.06	75.0	10.88	3.10	1.12	0.07	4.58	3.82	0.07	0.05	<0.01	0.005	99.79	44.33	53.23	41.45
ST 32		0.85	77.8	11.23	2.99	0.29	1.28	5.38	0.20	0.06	0.16	0.02	0.003	100.25	54.08	54.52	54.17
ST 33		0.21	75.5	11.27	3.04	0.20	0.04	5.31	3.68	0.05	0.18	<0.01	0.003	99.49	46.36	55.36	44.58
ST 36		0.65	79.2	7.55	1.88	0.15	0.16	0.35	5.56	0.01	0.19	0.01	0.003	95.76	52.49	89.91	65.16
ST 39		0.30	73.4	11.16	4.18	0.38	0.03	5.52	3.63	0.06	0.18	0.01	0.007	98.85	44.96	53.35	42.64
ST 1		0.68	74.1	11.63	3.66	0.75	0.29	4.51	3.69	0.03	0.16	<0.01	0.028	99.57	47.73	57.00	46.62

(Continues)

TABLE 2 (Continued)

Sample No. Unit MDL	Analyte	LOI % −5.11	SiO_2 % 0.1	Al_2O_3 % 0.01	Fe_2O_3 % 0.01	CaO % 0.01	MgO % 0.01	Na_2O % 0.01	K_2O % 0.01	MnO % 0.01	TiO_2 % 0.01	P_2O_5 % 0.01	Cr_2O_3 % 0.001	SUM % 0.01	CIA	CIW	PIA
ST 30	Felsite dikes	1.80	74.3	12.96	1.07	1.21	0.11	3.01	5.02	0.01	0.08	<0.01	0.006	99.59	50.81	64.47	51.42
ST 25		0.90	75.4	12.97	0.66	0.80	0.03	4.94	4.35	0.01	0.08	0.01	0.010	100.22	47.65	57.54	46.41
ST 26		0.96	75.9	12.78	0.51	0.89	0.04	5.80	2.67	<0.01	<0.01	<0.01	0.007	99.57	47.71	53.41	47.08
ST 27F		1.30	77.4	12.65	1.14	1.10	0.07	6.37	0.41	0.01	0.06	<0.01	0.003	100.52	49.54	50.37	49.53
ST 34	Pegmatite veins	0.22	75.2	10.96	4.21	0.28	0.02	5.21	3.69	0.05	0.05	<0.01	0.005	99.93	45.68	54.72	43.53
ST 35		0.25	76.1	10.58	3.70	0.22	<0.01	4.84	3.79	0.04	0.09	<0.01	0.004	99.65	45.99	55.88	43.77
SR-4F	Metavolcanics (dacite)	2.44	59.9	16.20	6.05	4.47	2.85	4.69	1.82	0.12	0.76	0.26	0.010	99.61	48.55	50.59	48.35
SR-4A		2.82	58.8	16.81	6.36	6.13	2.03	4.51	0.85	0.12	0.99	0.31	0.005	99.75	47.31	47.55	47.17
SR-5F		3.68	53.9	17.95	8.18	5.69	3.63	5.74	0.19	0.11	0.86	0.29	0.021	100.26	48.22	47.60	48.20
SR-5A		5.07	54.7	17.83	7.80	3.61	3.29	5.18	0.43	0.09	0.86	0.28	0.004	99.17	54.54	54.20	54.67
SR-8F		5.22	63.1	13.40	5.35	5.28	2.46	1.05	2.05	0.13	0.54	0.13	0.012	98.80	50.34	54.22	50.41
SR-8A		4.56	68.9	13.98	5.41	0.65	2.17	1.39	2.17	0.06	0.31	0.07	0.007	99.73	71.25	80.14	77.92
SR-11F		1.30	55.4	16.87	9.11	8.50	4.81	2.80	0.54	0.16	0.79	0.16	0.008	100.49	45.46	45.71	45.32
SR-11A		8.16	44.2	15.19	8.12	15.92	4.62	2.38	0.35	0.18	0.57	0.11	0.019	99.80	31.56	31.64	31.27
SR-12F		4.49	61.0	18.13	5.94	1.84	1.98	0.67	4.20	0.10	0.81	0.22	0.005	99.48	68.19	80.32	77.63
SR-35F		2.94	56.3	17.83	7.49	8.72	1.86	3.16	1.20	0.14	0.94	0.23	0.006	100.84	45.02	45.89	44.67
SR-37F		4.47	61.3	13.44	6.18	5.04	2.77	3.90	1.17	0.11	0.84	0.16	0.022	99.43	44.98	46.34	44.51
SR-37A		8.68	55.9	11.85	4.75	11.12	1.99	3.43	1.00	0.11	0.67	0.16	0.017	99.68	30.88	31.45	29.74
ST 16		2.86	50.9	16.85	8.02	12.50	5.49	2.96	0.24	0.17	0.66	0.09	0.043	100.77	37.90	37.94	37.76
ST 17		5.86	51.3	16.84	9.28	8.04	5.35	2.43	0.27	0.14	0.57	0.05	0.024	100.11	47.30	47.53	47.25
SR-22F		2.50	63.0	15.97	4.54	4.15	2.13	3.63	2.73	0.04	0.62	0.15	0.013	99.49	49.81	54.19	49.77
SR-22A		6.20	53.7	17.12	6.36	4.80	2.73	5.79	2.08	0.08	0.69	0.16	0.008	99.71	46.00	48.43	45.45
SR-26F	Metavolcanics (andesite)	5.06	54.6	14.79	6.63	4.99	8.01	3.51	1.42	0.11	0.88	0.19	0.050	100.20	48.18	49.93	47.97
SR-26A		3.85	56.4	18.58	5.98	4.20	4.30	5.81	0.40	0.12	0.72	0.19	0.017	100.57	52.00	51.97	52.05
SR-30F		13.89	48.9	9.91	4.11	14.98	3.23	2.74	0.81	0.29	0.60	0.18	0.019	99.69	23.56	23.81	22.41
SR-30A		15.89	45.0	9.88	4.35	16.60	3.63	2.70	0.81	0.23	0.62	0.17	0.018	99.89	21.99	22.22	20.85
SR-27F		6.62	35.6	16.30	17.78	10.60	10.68	0.20	0.27	0.28	1.76	0.14	0.081	100.25	45.49	45.43	45.41
SR-27A		13.79	41.7	1.70	7.45	0.72	34.31	0.20	0.10	0.13	0.08	0.01	0.297	100.17	49.70	50.96	49.68
ST 12A		6.79	59.7	15.34	5.79	5.12	2.12	0.40	3.40	0.14	0.71	0.19	<0.001	99.75	53.80	60.64	55.11
SR-31F		6.05	60.20	14.32	5.21	5.71	1.46	4.63	0.99	0.21	0.68	0.16	0.01	99.65	43.42	44.34	42.96

TABLE 2 (Continued)

Sample No.		LOI	SiO_2	Al_2O_3	Fe_2O_3	CaO	MgO	Na_2O	K_2O	MnO	TiO_2	P_2O_5	Cr_2O_3	SUM	CIA	CIW	PIA
Unit		%	%	%	%	%	%	%	%	%	%	%	%	%			
MDL	**Analyte**	**−5.11**	**0.1**	**0.01**	**0.01**	**0.01**	**0.01**	**0.01**	**0.01**	**0.01**	**0.01**	**0.01**	**0.001**	**0.01**			
SR-31A		8.03	60.70	13.58	5.54	4.74	2.18	2.42	1.44	0.15	0.68	0.16	0.00	99.64	49.68	51.90	49.63
SR-33F		3.08	63.30	14.56	5.81	3.43	2.92	4.03	1.42	0.09	0.80	0.18	0.03	99.62	51.06	53.12	51.19
SR-33A		6.57	52.80	14.98	8.82	6.75	5.36	1.20	1.60	0.14	1.04	0.29	0.02	99.63	49.53	51.29	49.47

Abbreviations: CIA, chemical index of alteration; CIW, chemical index of weathering; LOI, loss on ignition; PIA, plagioclase index of alteration.

reach 27,900 nGyh-1 as a maximum value over aplite-pegmatite and diminishes to 7 nGyh-1 over the metavolcanics of the Mahd Group.

The uranium and thorium maps (Figures 4b,c) are closely similar to the total dose rate map, that is, the highest radioactive zones, which are shown in the total dose rate map, could be traced from the uranium and thorium maps. The eU readings reach up to 1,550 ppm, whereas those of eTh reach up to 7,974 ppm. Figure 4d demonstrates a prominent K anomaly observed in the areas of aplite-pegmatite with an average concentration of 16.4%.

From an exploration point of view, the most important parameters that can be measured are the relative concentration of uranium to thorium and uranium to potassium taken in conjunction with the uranium measurements. These are diagnostic for identification of zones of anomalous uranium concentration (Darnley, 1973). All parts of the aplite-pegmatite and granitic rocks with high eU also have high eTh and show low eU/eTh values (<1) (Figure 4e). The eU/eTh ratio is about 0.33 in granitic rocks (Clark *et al*., 1966). Conversely, the metavolcanic of the Mahd Group has relatively high eU/eTh ratio values (up to 7). The eU/K contour map (Figure 4f) shows noticeable high anomalies (up to 40). This map demonstrates a significant agreement with the total dose rate, uranium, and thorium contour maps.

Results of gamma-ray spectrometric analyses of the study area are treated statistically to determine the minimum, maximum, arithmetic mean(X), *SD* (S), and coefficient of variability (CV%) (Table 1). Figure 5 shows the averages of total dose rate, eTh, eU, and K for the different rocks of the study area. Metavolcanics of the Mahd Group reflects the lowest radioactivity levels averaging 22.64 nGyh-1, 1.61 ppm, 0.84 ppm, and 0.92% for the total dose rate, eTh, eU, and K, respectively. Generally, the recorded low concentrations of the three radioactive elements eTh, eU, and K for the metavolcanics were found to be very close to the normal tabulated ranges for the different metavolcanics (Plant *et al*., 1999). Accordingly, these rocks are insignificant in terms of exploration of the natural radioactive elements, especially uranium. On the other hand, the aplite-pegmatite is marked by very high radioactivity levels averaging 7,773 nGyh-1, 1,841 ppm, 488.42 ppm, and 16.83% for the total dose rate, eTh, eU, and K, respectively. The alkali granite has total dose rate values ranging from 100 to 628 nGyh-1 with average of 205 nGyh-1, thorium values range from 11 to 126 ppm with average of 33.8 ppm, uranium values range from 5.1 to 42 ppm with average of 12.43 ppm and potassium concentration ranges from 1.4 to 4.9% with average of 3.72%. Such values for aplite-pegmatite and

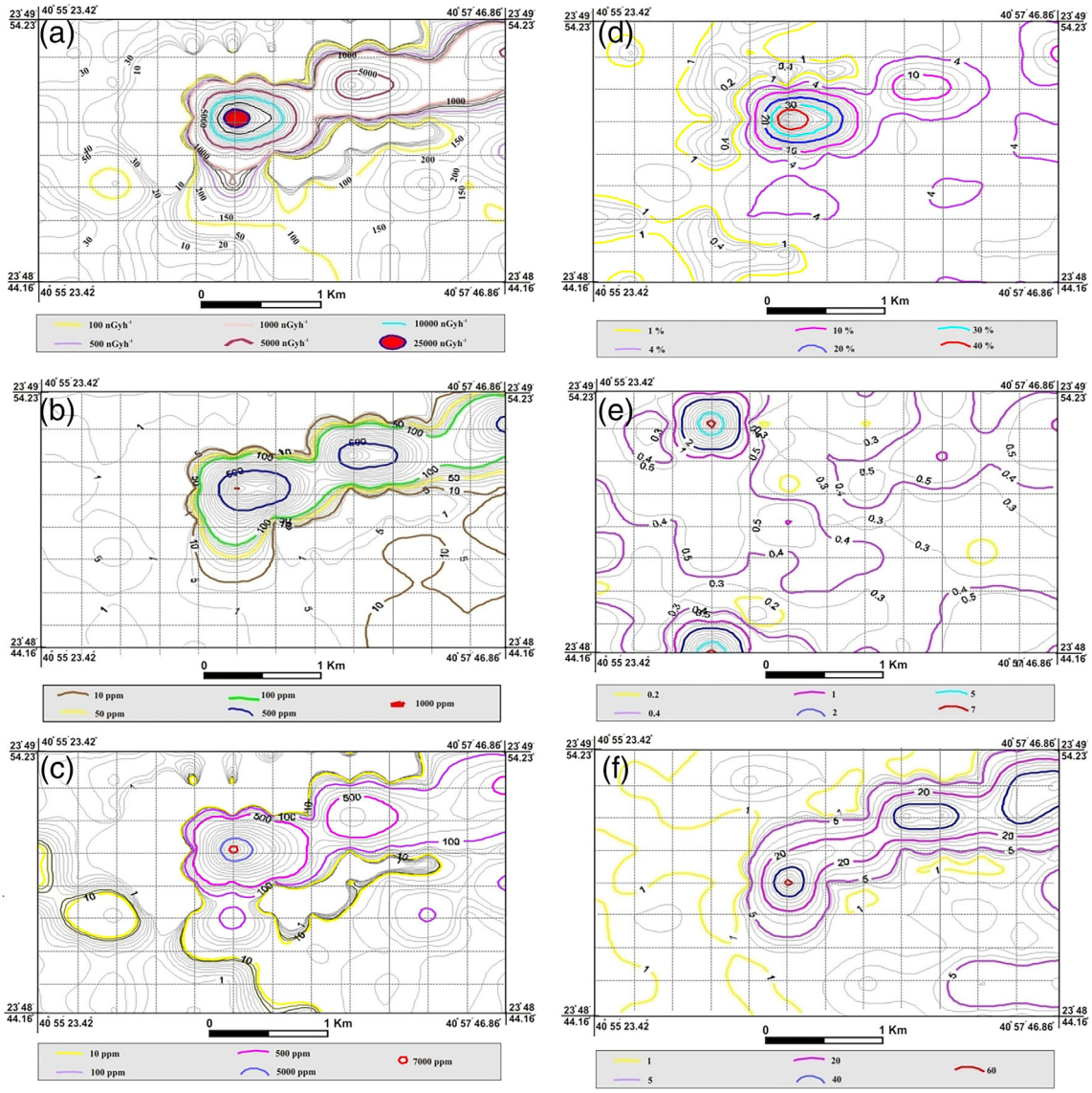

FIGURE 4 Contour maps showing the distribution of (a) total dose rate (nGyh-1), (b) eU (ppm), (c) eTh (ppm), (d) Potassium (%), (e) eU/eTh and (f) eU/K, in the Jabel Sayid area

alkali granite are agreeable with the conclusion of Ragland *et al.* (1967) that U and Th contents of granitic rocks generally increase during differentiation.

Wadi deposits close to the aplite-pegmatite and alkali granite reflects high radioactivity levels where total dose rate values range from 45 to 3,800 nGyh-1 with average of 698.13 nGyh-1, thorium values range from 4.9 to 1,051 ppm with average of 161.17 ppm, uranium values range from 1.8 to 164 ppm with average of 34.18 ppm and potassium concentration ranges from 1.1 to 4.2 % with average of 2.54 %. The highest values of the spectrometric results of Wadi deposits are close to Jabel Sayid pluton and decrease gradually away from the pluton in all directions. Microscopic study of heavy minerals mounts of some selected Wadi deposits close to the aplite-pegmatite and alkali granite indicate that zircon and thorite are the essential minerals responsible for the high radioactivity of these sediments (Figure 6).

The pegmatite veins within the granitic rocks of Jabel Sayid have total dose rate values ranging from 191 to 1,300 nGyh-1 with average of 510.75 nGyh-1, thorium values range from 19.3 to 273 ppm with average of 101.14 ppm, uranium values range from 10 to 96 ppm with average of 33.74 ppm and potassium concentration ranges from 4.1 to 5.9 % with average of 4.63 %. The felsite dikes within the alkali granite have total dose rate values that range from 107 to 578 nGyh-1 with average of 197.4 nGyh-1, thorium values range from 16.4 to 93 ppm with average of 32.35 ppm, uranium values range from 2.8 to 50 ppm with average of 10.95 ppm and potassium concentration ranges from 0.1 to 5.4 % with average of 3.87 %.

The standard formulation of the coefficient of variability (CV %), the ratio of the *SD* to the mean multiplied by 100, is applied on the four variables (total dose rate, eU, eTh, K) of each rock unit of Jabel Sayid area (Table 1). For a certain variable value, if the CV % is less than 100 %, the variable tends to exhibit normal distribution (Sarma and Koch, 1980), whereas the higher the CV %, the greater the dispersion in the variable. In the present study, the percentages of CV values of the four variables (total dose rate, eU, eTh, K) were graphically illustrated as a bar chart (Figure 7). From this table and bar chart, we can conclude that the four variables of the different rock units of the study area show normal distribution, where all the percentages of CV values are less than 100, with the exception of eU in felsite that shows CV % value slightly higher than 100 (Figure 7).

4.1.2 | Uranium mobilization

Uranium and thorium are strongly fractionated during magmatic processes and tend to be concentrated in the silicic/felsic part of a magma. This explains why they behave isochemically during magmatic processes. However, during weathering and other crustal processes, U^{4+} is easily oxidized to U^{6+}, which is soluble in groundwaters, whereas Th remains insoluble in the oxidization zone (Finch and Ewing, 1992). As a result, the eU/eTh ratio is highly affected by the oxidation processes that can lead to uranium migration and consequently its loss or gain. Therefore, the eU/eTh ratio is a geochemical parameter in the mobilization of uranium (Naumov, 1959). The commonly reported eU/eTh ratio for granitic rocks is about 0.33 (Clark *et al.*, 1966; Rogers and Adams, 1969; Stuckless *et al.*, 1977; Boyle, 1982). In the present study, the eU/eTh ratios specify recognizable variations among the investigated rocks (Table 1). The eU/eTh ratios of values less than 0.33 indicate limited mobilization of uranium from certain parts of the rock to other nearby parts in the same rock of more than 0.33 eU/eTh value. Moreover, the averages (0.43, 0.39, 0.4, and 0.31 for aplite-pegmatite, alkali granite, pegmatite veins, and felsite dikes, respectively) are generally

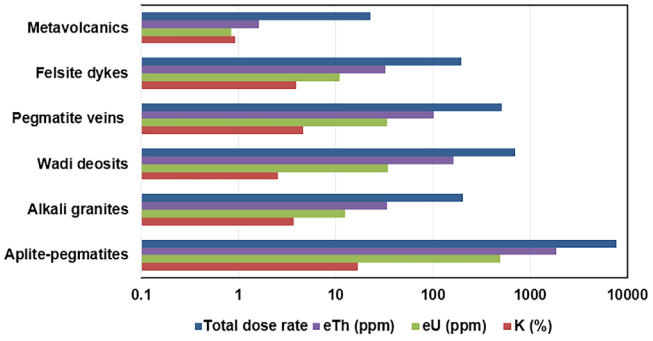

FIGURE 5 Averages of total dose rate, eTh, eU, and K for the different rocks of the Jabel Sayid area

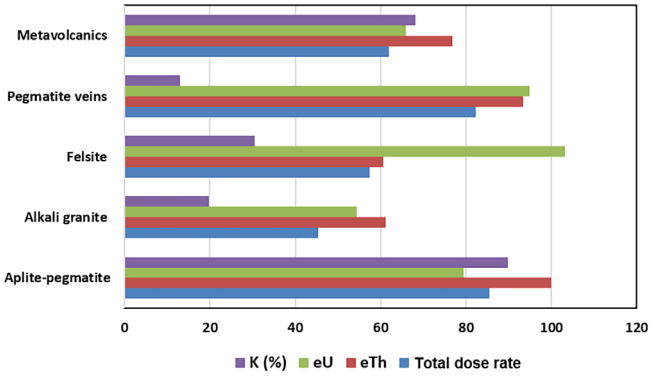

FIGURE 7 The percentages of CV values of the four variables (total dose rate, eU, eTh, K) for the different rocks of the Jabel Sayid area

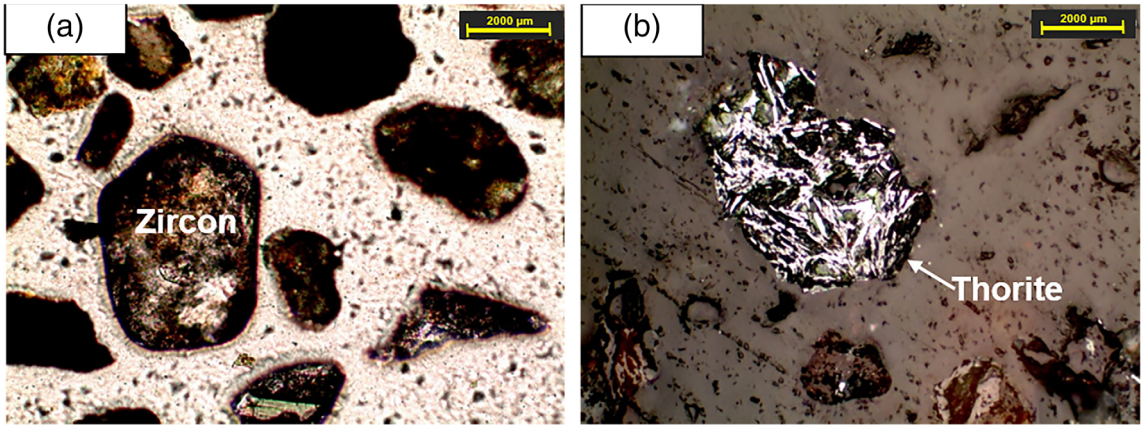

FIGURE 6 (a) Zircon under plane polarized light, (b) Thorite under polarized light

	eU – eTh	eU – eU/eTh	eTh – eU/eTh	eU – K	eTh – K
Aplite-pegmatite	0.806	−0.147	−0.683	0.852	0.920
Alkali granite	0.729	0.200	−0.453	0.136	0.289
Felsite dikes	0.779	0.765	0.283	−0.207	0.073
Wadi deposits	0.888	−0.196	−0.481	0.861	0.752
Pegmatite veins	0.707	0.492	−0.707	0.699	0.430
Metavolcanics	0.431	−0.048	−0.556	0.703	0.386

TABLE 3 Computed bivariate correlation coefficient matrix between the five radio-spectrometric variables of the different rocks in the Jabel Sayid area

around the previously reported value for granites supporting a limited redistribution of U over the Jabel Sayid pluton.

Correlation coefficients between eU, eTh, K, and eU/eTh of the different rocks are shown in Table 3. Relation between uranium and thorium is helpful to test if there is enrichment or depletion of these elements. eU is directly correlated with eTh in all rock varieties, except metavolcanics, which indicate that the uranium and thorium distribution is governed by the magmatic process. This interpretation is confirmed from the plot of the eU vs. the corresponding eTh values (Figure 8a). The significant Pearson's correlation coefficient between eU and eTh ($r = +0.615$) for these rock varieties reflects their geochemical coherence during the crystallization of magma and indicates that both elements are mainly accommodated into accessory minerals and were not disturbed by alteration.

With the exception of felsite dikes, the relation between eU and eU/eTh show a random distribution (Figure 8b). This means the eU/eTh ratio is not affected by late uranium mobilization and post magmatic redistribution in the studied rocks. On the other hand, the increase in eU with eU/eTh in felsite dikes indicates post magmatic remobilization of uranium (Figure 8b). The inverse correlation between eTh and eU/eTh ratio (Figure 8c) indicates that the radioelements distribution was at least partly governed by magmatic processes.

Bivariate diagrams eU-K and eTh-K plots (Figure 8d,e) show a uranium and thorium enrichment trend with increasing K contents for aplite-pegmatite and associated pegmatite veins. Such trend reflects radioelements enrichment with magmatic differentiation. Similar trend is also noticed for Wadi deposits close to aplite-pegmatites supporting the conclusion that most of uranium and thorium is accommodated in the accessory minerals. On the other hand, the scatter and/or ill-defined relation between eU-K and eTh-K for the alkali granites and felsite dikes (Figure 8d,e) may indicate postmagmatic redistribution of these elements. Limited mobilization, especially along fractured zones and quartz veins, is also documented by the presence of secondary minerals such as kasolite. Dawood *et al*. (2010) attributed the origin of secondary uranium mineralization in the Jabel Sayid area to hydrothermal fluids derived from the granitic magma. Redistribution by circulating meteoric water may have taken place as evidenced by widespread silicification, sericitization, and oxidation alteration.

The type and the amount of uranium mobilization in the studied rocks are estimated through several steps using equations of Benzing Uranium Institute of China (1977) and CNNC (1993)), these equations are examined by several authors (Abu-Deif *et al*., 2001; Asfahani *et al*., 2007, 2010, 2016; Assran *et al*., 2012; Attia and Shendi, 2013) as follows:

$$U0 = eTh * eU/eTh,$$

where U0 is the original uranium content, eTh is the average of the equivalent thorium content in certain geological unit in ppm and eU/eTh is the average of regional eU/eTh ratio in different geological units.

$$Um = Up - U0$$

where Um is the amount of the mobilized uranium and Up is the average of the present uranium content in certain geologic unit. Two states of Um are expected; (a) if $Um > 0$, U could be gained or mobilized into the geologic body during late evolution (migration in) and (b) if $Um < 0$, U could be lost from the geologic body during late evolution (migration out).

$$P = Um/Up * 100,$$

where, P is the uranium migration rate. The P % is a good indicator for determining the migration degree and its direction. Negative P % values indicated movement of U out of the region, while positive P % indicated movement into a region.

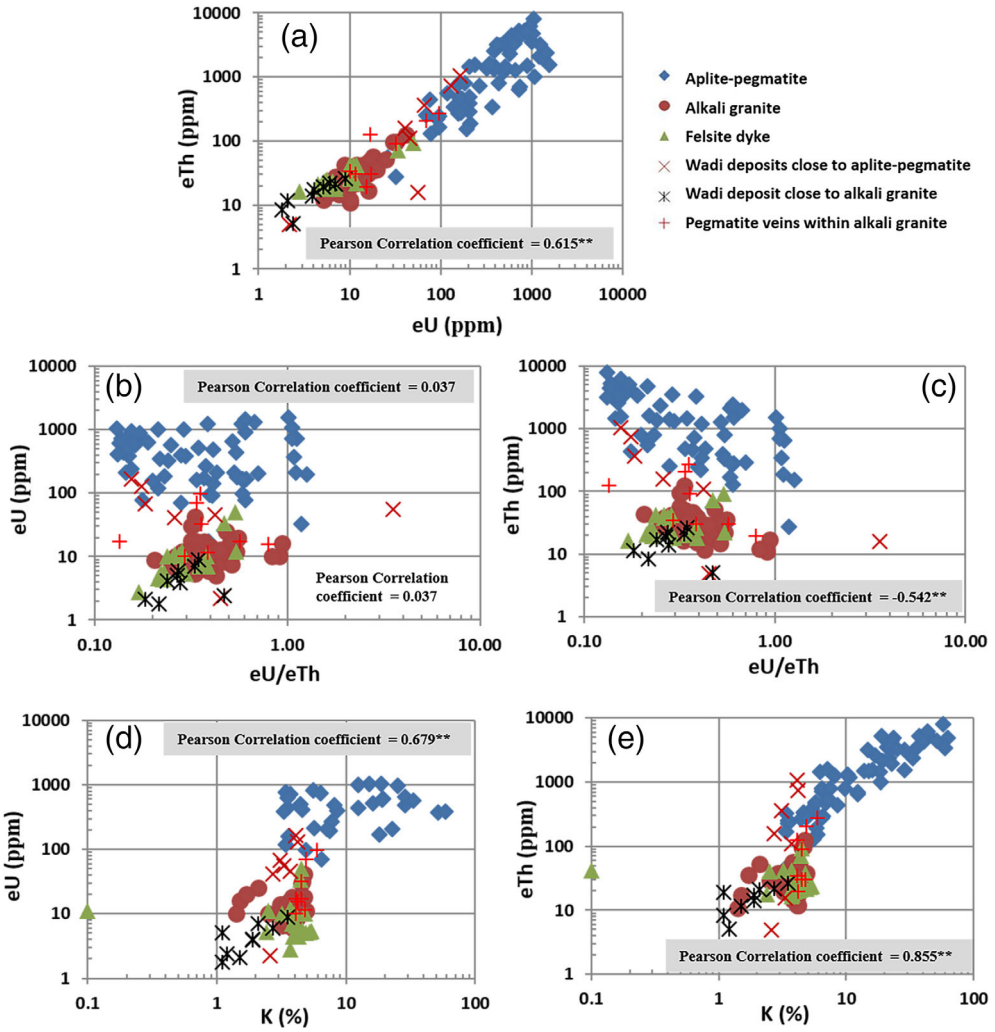

FIGURE 8 Binary diagrams showing (a) eU vs. eTh, (b) eU vs. eU/eTh, (c) eTh vs. eU/eTh, (d) K vs. eU, and (e) K vs. eTh, in the different lithologies in the Jabel Sayid area. ** Correlation is significant at the 0.01 level (2-tailed)

In the study area, the uranium migration rate is computed for the different rock units (Table. 4). According to these values, all geological rock units in the study area have been identified as uranium-source rocks, with the exception of the felsite dikes. The aplite-pegmatite has the highest uranium outward migration with the migration rate of −62.08%. It is followed by pegmatitic veins and alkali granite that have migration rates of −19.91 and −6.05%, respectively. The high rate of migration of these rocks may indicate that they represent the main uranium-source rock in the study area. Conversely, felsite dikes show positive value of uranium inward migration (0.92) with the migration rate of 8.42%. This rate of migration strongly implies that this rock is probably the main rock receiving uranium in the study area.

4.1.3 | Uranium Favorability

In the present study, uranium favorability indices U_1 and U_2 developed by Saunders and Potts (1978) are used. U_1 is defined as the ratio of all increasing parameters to all decreasing parameters and is given by the following relationships:

$$U_1 = \frac{(\mathrm{MeU} + \mathrm{MeTh} + \mathrm{MK}) * \mathrm{RSDeU} * \mathrm{RSD(eU/eTh)} * \mathrm{RSD(eU/K)}}{\mathrm{M(eU/eTh)} * \mathrm{M(eU/K)}},$$

where M refers to the mean value, RSD means relative *SD*. In some cases, the coefficient of variability (CV) and the RSD are the same thing. The same authors suggested a simpler equation for the second uranium favorability index (U_2) that is expressed with the following equation:

$$U_2 = \mathrm{M\,eTh} * \mathrm{MK/MeU}.$$

Table 5 shows uranium favorability indices U_1 and U_2 for the different rocks in the study area. It indicates that aplite-pegmatite is the most favorable for uranium, followed by pegmatite veins, felsite dikes and alkali granite, respectively. Metavolcanics is the least favorable rock

TABLE 4 Mean values of the present uranium, original uranium, uranium migration extent, and direction of uranium migration for the different rocks in the study area

Rock type	No. of samples	Present uranium (Up)	Original uranium content (U_0)	Uranium migration (Um)	Uranium migration rate (P)	Direction of migration
Aplite-pegmatite	64	488.42	791.63	−303.21	−62.08	Out
Alkali granite	56	12.43	13.182	−0.752	−6.05	Out
Wadi deposits	16	34.18	78.9733	−44.7933	−131.05	Out
Pegmatite veins	8	10.95	40.456	−6.716	−19.91	Out
Felsite dikes	20	33.74	10.0285	0.9215	8.42	In
Metavolcanics	13	0.84	1.7871	−0.9471	−112.75	Out

TABLE 5 uranium favorability indices U_1 and U_2 for the different rocks in the Jabel Sayid area

Rock type	N	M eU	M eTh	M K (%)	RSD eU	RSD eU/eTh	RSD eU/K	M eU/eTh	M eU/K	U1	U2
Aplite-pegmatite	64	488.42	1,841	16.83	79.41	72.09	52.45	0.43	32.68	50,134,714	63.44
Alkali granite	56	12.43	33.8	3.72	54.47	35.90	66.85	0.39	3.59	4,663,094	10.12
Felsite	20	10.95	32.35	3.87	103.11	35.48	297.78	0.31	8.1	20,465,495	11.43
Pegmatite veins	8	33.74	101.14	4.63	94.93	50.00	80.85	0.4	6.79	19,713,331	13.88
Metavolcanics	132	0.84	1.61	0.92	66.67	188.29	51.38	0.49	1.09	4,069,124	1.76

Abbreviations: M, mean value; RN, number of samples; SD (relative standard deviation) = 100 * S /M, where S refers to standard deviation.

for uranium in the study area. Although the aplite-pegmatite, alkali granite, and the associated pegmatite veins show negative value of uranium outward migration (Table 4), they are still favorable rocks for uranium in the study area. A tentative interpretation of such contradiction suggests that uranium is largely accommodated into accessory minerals and a limited labile uranium redistribution has occurred and uranium may be reconcentrated with silicification, sericitization, and oxidation products. The expected original uranium is calculated by dividing the measured eTh by the average Th/U ratio in the crustal acidic rocks, that is, original uranium = eTh/3.5 (Abdel Meguid *et al*., 2003; Abouelnaga *et al*., 2015). The result of these calculations is subtracted from the measured eU and represented graphically in the form of contour map (Figure 9). Positive values indicate uranium addition by mobilization, whereas negative values indicate migration of uranium from these places. From Figure 10, it is noticed that positive values (green colour) are concentrated along the aplite-pegmatite and oxidized alkali granites where quartz and pegmatite veins are abundant.

4.2 | Geochemical study

Chemical weathering indices are commonly used to describe the features of the different weathering rocks through the integration of major oxide elements in one metric scale for each sample. Generally, in homogeneous parent rocks, weathering indices are changed with depth. However, the weathering of heterogeneous metamorphic rocks confounds the relationship between weathering index and depth (Price and Velbel, 2003). All weathering indices are based on the calculated ratios of immobile elements against the other mobile elements. Aluminum is always an immobile element, while the mobile elements are mainly calcium, potassium, sodium, and in some cases iron is added. For example, Chemical Index of Alteration, or CIA (Nesbitt and Young, 1982), Chemical Index of Weathering, or CIW (Harnois, 1988) and Plagioclase Index of Alteration, or PIA (Fedo *et al*., 1995), are three weathering indices that are represented by the following equations:

$$\mathrm{CIA} = (\mathrm{Al_2O_3}/(\mathrm{Al_2O_3} + \mathrm{CaO^*} + \mathrm{Na_2O} + \mathrm{K_2O}) \times 100$$

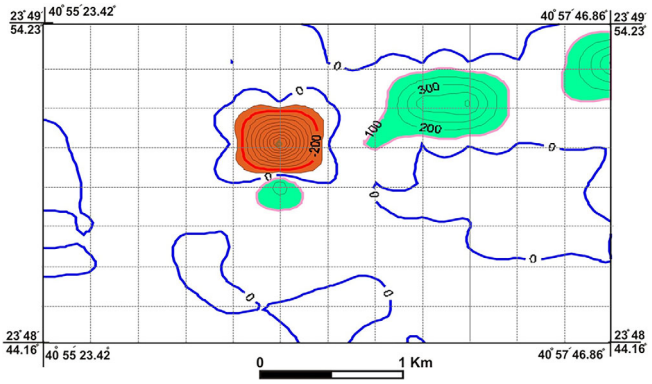

FIGURE 9 Contour map showing the distribution of original uranium (original uranium = eTh/3.5) in the Jabel Sayid area

$$CIW = (Al_2O_3/(Al_2O_3 + CaO^* + Na_2O) \times 100$$

$$PIA = [(Al_2O_3 - K_2O)/(Al_2O_3 + CaO^* + Na_2O - K_2O) \times 100)]$$

where CaO* represents only calcium oxide in silicate minerals (mainly in plagioclase), this means excluding all non-silicate calcium oxides. In igneous rocks (except carbonitites), apatite $[Ca_5(PO_4)_3]$ is the most abundant non-silicate calcium bearing mineral, so the following equation is used to do the required correction of the non-silicate calcium:

$$\text{mol CaO} * = \text{molCaO} - 10/3 \text{ mol } P_2O_5$$

CIA, CIW, and PIA indices are calculated for the different rocks in the study area. The calculated values are compared with the corresponding values of the unweathered rocks.

4.3 | A–CN–K diagram

The molecular weights of the oxides of the studied rocks are represented on the A-CN-K diagram after Nesbitt and Young (1984, 1989) in order to understand the chemical weathering trends of these rocks (Figure 10a). The ends of this diagram are the variables used in the calculation of CIA. Generally, the CIA for unweathered rocks is close to 50, whereas values less than 60 represent weak weathering rate, while values of 60–80 represent moderate weathering rate, and values above 80 represents high weathering rates (Fedo *et al.*, 1995). The CIA values for the different rock units in the study area are shown in Table 2. In general, the rocks of Jabel Sayid area could be considered as unweathered, with the exception of few samples of low to medium weathering (Figure 10a).

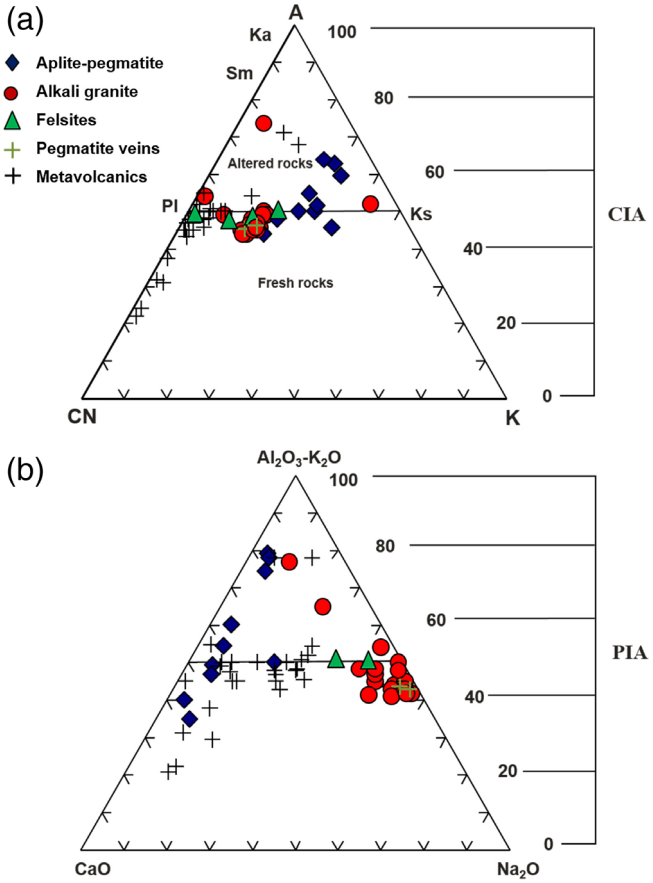

FIGURE 10 (a) Ternary plot showing the chemical index of alteration (CIA) in the different lithologies of the Jabel Sayid area. Where: A = Al_2O_3, CN = (CaO* + Na_2O), K = K_2O, Pl = plagioclase, Ks = K-feldspar, Ka = kaolinite, Sm = Smectite. (b) Ternary plot showing the plagioclase index of alteration (PIA) in the different lithologies in the Jabel Sayid area

4.4 | A–C–N diagram

Plagioclase alteration can add more information about weathering of the silicate minerals in the studied rocks. Fedo *et al.* (1995) designed the A-C-N diagram that depends on the molecular ratios of aluminum oxide (after subtracting the aluminum value associated with potassium in K-feldspar mineral), calcium oxide, and sodium oxide. Plagioclase index of alteration (PIA) is based on the following equation:

$$PIA = [(Al_2O_3 - K_2O)/(Al_2O_3 + CaO* + Na_2O - K_2O) \times 100)].$$

The PIA values of the studied rocks are shown in Table 2. These values agree well with the results of CIA, which indicates unweathered rocks, with the exception of few samples that showed low to medium weathering (Figure 10b).

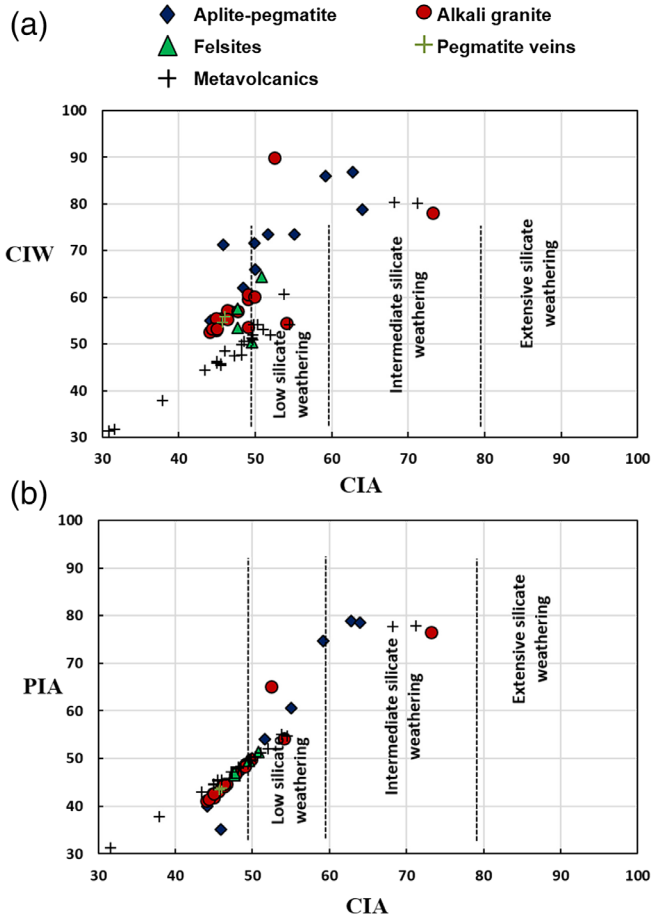

FIGURE 11 Binary diagrams showing (a) CIA vs. CIW, (b) CIA vs. PIA, in the different lithologies in the Jabel Sayid area

Figure 11a,b shows bivariate relations between the CIA and both of CIW and PIA. It shows a linear relationship between these indices indicating low weathering rates in general and consequently a limited role of weathering processes in the mobility of uranium in the Jabel Sayid area.

5 | CONCLUSIONS

The Jabel Sayid area was investigated for the purpose of identification and assessment of natural radioelements distribution. The spectrometric survey revealed the presence of three enriched zones related primarily to the aplite-pegmatite. The average eU content of the investigated rocks varies, the aplite-pegmatite is 488 ppm (range: 17–1,550 ppm), the alkali granite is 12 ppm (range: 5–42 ppm), the felsite dikes is 11 ppm (range: 3–50 ppm), the pegmatite veins in alkali granite is 34 ppm (range: 10–96 ppm), and the Mahd volcanics is 0.8 ppm (range: 0–2 ppm). The relatively low eU/eTh ratios in both the aplite-pegmatite and the alkali granite (<1) indicate a limited post magmatic redistribution processes, where these values are comparable to the average of granites (0.25) as reported by Adams *et al*. (1959).

Uranium favorability indices U_1 and U_2 for the different rocks in the study area indicate that aplite-pegmatite is the most favorable for uranium, followed by pegmatite veins, felsite dikes, and alkali granite, respectively. Whereas, metavolcanics are the least favorable rock for uranium. The uranium mobility was attenuated due to absorption by iron oxides and clay minerals in the same rock. This is supported by the occurrence of uranyl minerals associated with goethite and argillic alteration products in the interstitial fractures adjacent to the small pegmatite and quartz veins (Dawood *et al*., 2010). Chemical index of alteration (CIA), chemical index of weathering (CIW), and plagioclase index of alteration (PIA) showed low weathering rates for the different rocks of the study area and reflecting the limited role of weathering processes in the mobility of the elements in these rocks.

ACKNOWLEDGMENTS

Our thanks are due to King Abdulaziz City for Science and Technology (KACST(for funding this project (Grant No. AT-30-31). Faculty of Earth Sciences, King Abdulaziz University is truly acknowledged for offering the laboratory facilities and organizing field trips.

DATA AVAILABILITY STATEMENT

Data openly available in a public repository that does not issue DOIs.

ORCID

Hamdy H. Abd El-Naby https://orcid.org/0000-0002-5211-6887

REFERENCES

Abdel Meguid, A.A., Cuney, M., Ammar, S.E., Ibrahim, T.M.M., Ali, K. h. G., Shahin, H.A., Omer, S.A., Gaafar, I.M., Masoud, S. M., Khamis, A.A., Haridy, M.H., Kamel, A.I., Mostafa, M.B., Abu Donia, A.M.H., Abdel Gawad, A. and Aly, E.M., (2003) *Uranium potential of Eastern Desert Granites. Egypt*. Internal report, NMA, Cairo, Egypt.

Abouelnaga, H.S.O., El-Shayeb, H., Mahmoud, T., Gaafar, I. and Abu Donia, A. (2015) Ground geophysical survey for studying the potentiality of uranium mineralization in rhyolite zone-Um Safi area, Central Eastern Desert, Egypt. *Arabian Journal of Geosciences*, 8, 6279–6303.

Abu-Deif, A., Abouelnage, H.S.O. and Hassanein, I.E. (2001) Distribution of radioelement and its relation to uranium migration, El-Erediya exploration tunnels, central eastern desert, Egypt. *Journal of King Abul Aziz University, Earth Science*, 13, 19–40.

Adams, J.A.S., Osmond, J.K. and Rogers, J.J.W. (1959) The geochemistry of thorium and uranium. In: Ahrens, L.H. (Ed.) *Physics and Chemistry of the Earth*, Vol. 3. London: Pergamon Press, pp. 298–348.

Asfahani, J., Aissa, M. and Al-Hent, R. (2007) Uranium migration in sedimentological phosphatic environment in northern Palmyrides, Al-Awabed Area, Syria. *Applied Radiation and Isotopes*, 65, 1078–1086.

Asfahani, J., Aissa, M. and Al-Hent, R. (2010) Aerial spectrometric survey for localization of favorable structures for uranium occurrences in Al-Awabed area and its surrounding (Area-3), Northern Palmyrides–Syria. *Applied Radiation and Isotopes*, 68, 219–228.

Asfahani, J., Al-Hent, R. and Aissa, M. (2016) Uranium remobilization and migration evaluation through aerial spectrometric gamma technique in Syrian Desert (Area-1), Syria. *Applied Radiation and Isotopes*, 107, 278–292.

Assran, A.S.M., Abdelhadim, H.M., El Shayeb, H.M., Ashami, A.S. and Zaeimah, M.A. (2012) Ground gamma-ray spectrometric study and environmental impact for Moreid-Elsahu Area, Southwestern Sinai, Egypt. *Arab Journal of Nuclear Sciences and Applications*, 45(2), 240–253.

Attia, T.E. and Shendi, E.H. (2013) Uranium migration history in the igneous and metamorphic rocks of Solaf-Umm Takha area, based on multi-variate statistical analysis and favourability indices, central south Sinai, Egypt. *IOSR Journal of Applied Geology and Geophysics*, 1, 09–20.

Benzing Uranium Institute of China (1977) Field Gamma-Ray Spectrometric Survey No. 3, 1-292, China.

Boyle, R.W. (1982) *Geochemical Prospecting for Thorium and Uranium Deposits* (1st ed, Vol. 16). Amsterdam: Elsevier Scientific Publishing Company. 508p. https://www.elsevier.com/books/geochemical-prospecting-for-thorium-and-uranium-deposits/boyle/978-0-444-42070-1.

Calvez, J.-Y., Alsac, C., Delfour, J., Kemp, J. and Pellaton, C. (1983) *Geologic evolution of western, central and eastern parts of the northern Precambrian Shield, Kingdom of Saudi Arabia*. Saudi Arabian Deputy Ministry for Mineral Resources Open-file Report BRGM-OF-03-17, 57 p.

Camp, V.E. and Roobol, M.J. (1989) The Arabian continental alkali basalt province: Part I. Evolution of Harrat Rahat, Kingdom of Saudi Arabia. *Geological Society of America Bulletin*, 101, 71–95.

China National Nuclear Corporation, CNNC. (1993) *Research achievement from Bureau of Geology*. Internal report, China.

Clark, S.P., Peterman, Z.E. and Heier, K.S. (1966) Abundance of uranium, thorium and potassium. *Geological Society of America Memoirs*, 97, 521–541.

Coleman, R.G., Gregory, R.T. and Brown, G.F. (1983) *Cenozoic volcanic rocks of Saudi Arabia*. U.S. Department of the Interior, Geological Survey, Open-File Report 83–788, 244p.

Darnley, A.G. (1973) *Airborne gamma-ray survey techniques - present and future*. IAEA, Vienna, Austria, Panel proceedings series, pp. 67-106.

Dawood, Y.H., Harbi, H.M. and Abd El-Naby, H.H. (2010) Genesis of kasolite associated with aplite-pegmatite at Jabel Sayid, Hijaz region, Kingdom of Saudi Arabia. *Journal of Asian Earth Sciences*, 37, 1–9.

Dawood, Y.H., Abd El-Naby, H.H. and Ghaleb, B. (2014) U-series isotopic composition of kasolite associated with aplite-pegmatite at Jabel Sayid, Hijaz region, Kingdom of Saudi Arabia. *Arabian Journal of Geosciences*, 7, 2881–2892.

Drysdall, A.R. and Douch, C.J. (1986) Nb-Th-Zr Mineralization in microgranite-microsyenite at Jabal Tawlah, Midyan region, Kingdom of Saudi Arabia. *Journal of African Earth Sciences*, 4, 275–288.

Fedo, C.M., Nesbitt, H.W. and Young, G.M. (1995) Unraveling the effects of potassium metasomatism in sedimentary rocks and paleosols, with implications for paleoweathering conditions and provenance. *Geology*, 23, 921–924.

Finch, J.R. and Ewing, C.R. (1992) The corrosion of uraninite under oxidizing conditions. *Journal of Nuclear Materials*, 190, 133–156.

Hackett, D. (1984) *Jabel Sayid rare earth prospect: drilling results and resource evaluation*. Saudi Arabian Deputy Ministry for Mineral Resources Open-File Report DGMR-OF-04-26.

Hackett, D. (1986) Mineralized aplite-pegmatite at Jabel Sayid, Hijaz region, Kingdom of Saudi Arabia. *Journal of African Earth Sciences*, 4, 257–267.

Hamath Ba, M., Jaffal, M., Lo, K., Youbi, N., Dahmada, M. E., Ibouh, H., Boumehdi, M. A., Aïfa, T., Amara, M., Jessell, M., Ernst, R. E., Bensalah, M. K., and Söderlund, U. (2020) Mapping mafic dyke swarms, structural features, and hydrothermal alteration zones in Atar, Ahmeyim and Chami areas (Reguibat Shield, Northern Mauritania) using high-resolution aeromagnetic and gamma-ray spectrometry data. *Journal of African Earth Sciences*, 163, 103749. https://doi.org/10.1016/j.jafrearsci.2019.103749.

Hargrove, U.S. (2006) *Crustal evolution of the Neoproterozoic Bi'r Umq suture zone, Kingdom of Saudi Arabia: Geochronological, isotopic, and geochemical constraints*. Thesis, University of Texas at Dallas, UMI Number: 3225070.

Harnois, L. (1988) The CIW index: A new chemical index of weathering. *Sedimentary Geolgy*, 55, 319–322.

International Atomic Energy Agency (IAEA) (2010) *Radioelement Mapping*. IAEA Nuclear Energy Series, No. NF-T-1.3, Vienna, Austria, 108p.

Jiashu, R. and Zehong, H. (1982) Forms of Uranium occurrence and its distribution in uraniferous granites. In: Keqin, X. and Guangchi, T. (Eds.) *Geology of Granites and Their Metallogenetic Relations*. Beijing: Sciences Press, pp. 621–635.

Küster, D. (2009) Granitoid-hosted Ta mineralization in the Arabian–Nubian Shield: Ore deposit types, tectono-metallogenetic setting and petrogenetic framework. *Ore Geology Reviews*, 35(1), 68–86.

Luce, R.W.; O'Neil, J.R. and Rye, R.O. (1979) *Mahd Adh Dhahab: Precambrian epithermal gold deposit, Kingdom of Saudi Arabia*. USGS Open-File Report 79–1190, 33p. https://doi.org/10.3133/ofr791190

Moghazi, A.M., Iaccheri, L.M., Bakhsh, R.A., Kotov, A.B. and Ali, K.A. (2015) Sources of rare-metal-bearing A-type granites from Jabel Sayed complex, Northern Arabian Shield, Saudi Arabia. *Journal of Asian Earth Sciences*, 107, 244–258.

Moufti, M.R.H. (1985) *The Geology of Harrat Al Madinah Volcanic Field, Harrat Rahat, Saudi Arabia*. Thesis, University of Lancaster, U.K., 522p. http://hdl.handle.net/10068/619962

Naumov, G.B. (1959) Transportation of uranium in hydrothermal solution as carbonate. *Geochemistry*, 1, 5–20.

Nesbitt, H.W. and Young, G.M. (1982) Early Proterozoic climates and plate motions inferred from major element chemistry of lutites. *Nature*, 199, 715–717.

Nesbitt, H.W. and Young, G.M. (1984) Prediction of some weathering trends of plutonic and volcanic rocks based on thermodynamic and kinetic considerations. *Geochimica Cosmo chimica Acta*, 48, 1523–1534.

Nesbitt, H.W. and Young, G.M. (1989) Formation and diagenesis of weathering profiles. *Journal of Geology*, 97, 129–147.

Pellaton, C. (1981) *Geologic map of the Al Madinah Quadrangle, sheet 24D*. Ministry of Petroleum and Mineral resources. Geologic map GM-52C, scale 250,000.

Plant, J.A., Simpson, P.R., Smith, B. and Windley, B.F. (1999) Uranium ore deposits-Products of the radioactive Earth. In: Burns, P. C. and Finch, R. (Eds.) *Uranium: Mineralogy, Geochemistry and the Environment. Reviews in Mineralogy*, Vol. 38. Washington, DC: Mineralogical Society of America, pp. 255–319.

Price, R.J. and Velbel, M.A. (2003) Chemical weathering indices applied to weathering profiles developed on heterogeneous felsic metamorphic parent rocks. *Chemical Geology*, 202(3–4), 397–416.

Ragland, P.C., Billing, G.K. and Adams, J.A.S. (1967) Chemical fractionation and its relationship to the distribution of thorium and uranium in a zoned granite batholith. *Geochimica et Cosmochimica Acta*, 31, 17–33.

Rogers, J.J.W. and Adams, J.A.S. (1969) Uranium and thorium. In: Wedepohl, K.H. (Ed.) *Handbook of Geochemistry*. Berlin: *Springer Verlag*, pp. 92-B-1–92-0-8 and 90-Bb-1 to 90–00-5.

Sarma, D.D. and Koch, G.S. (1980) A statistical analysis of exploration geochemical data for uranium. *Mathematical Geology*, 12, 99–114.

Saunders, D.F. and Potts, M.J. (1978) *Manual for Application of NURE1974–1977 Aerial Gamma-ray Spectrometric data*. U.S. Department of Energy, Grand Junction office, Report GJBX–13 (87), 183p.

Shives, R. (2017) Gamma ray spectrometry: exploration, environment, health and safety. In: *Minerals North Conference*, Prince George Conference and Civic Centre, Canada, April 26, 2017.

Stuckless, J.S., Bunker, C.M., Bush, C.A., Doering, W.P. and Scott, J.H. (1977) Geochemical and petrologic studies of auraniferous granite from the Granite Mountains, Wyoming. *U. S. Geological Survey Journal of Research*, 5, 61–81.

Turkistany, A.R.A. (1979) *Radioactive pegmatite and its host granites of Jabel Sayid, Saudi Arabia*. M.Sc. Thesis (unpublished), King Abdulaziz University, Jeddah.

Turkistany, A.R.A. and Ramsay, C.R. (1982) Mineralized apogranite associated with alkali granite at Jabel Sayid, Kingdom of Saudi Arabia. *Saudi Arabian Deputy Ministry for Mineral Resources Professional Paper*, 1, 79–88.

How to cite this article: Abd El-Naby HH, Dawood YH, Sabtan AA, Al Yamani MS. Significance of radioelements distribution in the Precambrian rocks of Jabel Sayid, western Saudi Arabia, using spectrometric and geochemical data. *Resource Geology*. 2020;1–18. https://doi.org/10.1111/rge.12253